PROCEEDINGS OF SCIENCE

First GERDA results on $0\nu\beta\beta$ decay of ^{76}Ge

Carla Maria Cattadori*on behalf of the GERDA collaboration
INFN Milano Bicocca
E-mail: carla.cattadori@lngs.infn.it

From November 2011 to May 2013, GERDA searched for $0\nu\beta\beta$ and $2\nu\beta\beta$ of ^{76}Ge. Eight semi-coaxial (COAX) Ge detectors enriched up to ∼86% in ^{76}Ge (^{enr}Ge) from the former Heidelberg-Moscow (HDM) and Igex (IGEX) experiments and later 5 freshly produced ^{enr}Ge *button*-contact detectors (BEGE), for a total mass of ∼ 18 kg of ^{enr}Ge, were operated bare in liquid Argon, in the GERDA apparatus. A total exposure of 21.6 kg·yr of ^{enr}Ge has been collected in 492.3 days live time, allowing to scrutinize the existing claim of $0\nu\beta\beta$ evidence. GERDA did not observe any excess of events above the background at $Q_{\beta\beta}$ or in its immediate surroundings; the limit of $T^{0\nu}_{1/2} > 2.1 \cdot 10^{25}$ yr (90 % C.L.) is derived [1]. When combining the GERDA limit with those of past HDM and IGEX experiments, $T^{0\nu}_{1/2} > 3.0 \cdot 10^{25}$ yr (90 % C.L.). GERDA showed that its apparatus allows to operate Ge detectors achieving a background index (BI) of about 2.0 10^{-2} cts/(keV·kg·yr) and 1.0 10^{-2} cts/(keV·kg·yr) at $Q_{\beta\beta}$ (2039 keV), prior and after the pulse shape cuts respectively. The background is so low, that the $2\nu\beta\beta$ spectrum is clearly visible at energies < 1800 keV: the $T^{2\nu}_{1/2}=(1.84^{+0.14}_{-0.10}) \cdot 10^{21}$ yr was derived on a first data set corresponding to 5.1 kg·yr exposure [2]. In this contribution, the apparatus performances, the data reduction and treatment procedures, the main components of the residual background relevant to the $0\nu\beta\beta$ analysis, and the GERDA Phase I physics results are presented.

The European Physical Society Conference on High Energy Physics -EPS-HEP2013
18-24 July 2013
Stockholm, Sweden

*Speaker.

PoS(EPS-HEP 2013)515

1. Introduction

$0\nu\beta\beta$ and $2\nu\beta\beta$ predictions and experimental searches have a long lasting history. It starts in '30s with Goeppert-Mayer's and Furry's models, follows in the '60s with the first direct experimental searches, up to nowaday. $0\nu\beta\beta$ is a nuclear process forbidden in Standard model but allowed in some of its extensions. It is a test bench to probe the violation (by two units) of the so-far non violated lepton number conservation law, neutrino Majorana nature and of its absolute mass. In the last decade, with the evidence of neutrino flavour oscillation and the measurement of all the 3 relevant mixing angles and mass eigenvalues differences, $0\nu\beta\beta$ experimental searches revitalized leading to several new experimental projects. $0\nu\beta\beta$ can provide the missing informations in the neutrino sector namely the absolute mass scale (i.e. what is the mass of the lightest mass eigenvalue), the mass hierarchy (degenerate $m_1 \approx m_2 \approx m_3$ or hierarchical $m_1 < m_2 \ll m_3$ or $m_3 \ll m_1 < m_2$), the determination of the Majorana/Dirac nature of the neutrino, and the value of the effective Majorana neutrino mass (m_{ee}) [3][4][5]. Due to possible phase cancellations m_{ee} could be smaller than the lightest neutrino mass eigenvalue.
So far $2\nu\beta\beta$, a second order allowed process in Fermi theory, has been both directly and indirectly observed for twelve nuclei, (^{48} Ca, ^{76} Ge,^{82} Se,^{96}Zr, ^{100}Mo,^{116}Cd,^{128}Te,^{130}Te, ^{136}Xe, ^{150}Nd and ^{238}U), with half-lives ranging in the 10^{19}-10^{21} years[6]; it provides important constraints on nuclear matrix elements (NME). In fact for ^{76}Ge the NME$_{0\nu\beta\beta}$ ranging from 3.3 (Shell Model) to 6.5 (Intermediate Boson Model) represent the largest theoretical uncertainty on the expected $T^{0\nu}_{1/2}$[4]: the spread of values depends mainly from the adopted nuclear model but also on the computation methodics.
Evidences of $0\nu\beta\beta$ decay was never reported, but in 2004 when Klapdor et al. a subgroup of the HDM authors claimed indications [7] and then in 2006 evidence [8] for $0\nu\beta\beta$. This results was and is still largely debated in the community, because of data treatment issues [9] or missing informations. The GERDA collaboration formed in 2004[10], and the project got funds by the respective agencies in 2005, with three ambitious goal; *i)* build a setup allowing to reach, in the Ge detectors, a background index (BI) of 10^{-3} cts/(keV·kg·yr) at $Q_{\beta\beta}$= 2039 keV, *ii)* scrutinize, within two years, the claim, using the same isotope (^{76}Ge), and the same detectors of the completed HDM [12] and IGEX [13] experiments, while heavily modifying the detector environment, *iii)* after the completion of point *i)* add ~20 kg of new ^{enr}Ge detectors , with improved event topology reconstruction, to further reduce the background and improve the sensitivity on the $0\nu\beta\beta$ process half-live. To accomplish *i)* and *ii)* the GERDA setup is coincieved as described in [14] following an idea of G. Heusser et al. [11] and basically is a sequence of shells of increasing radiopurity to abate the environmnental radioactivity down to < 10^{-3} cts/(keV·kg·yr)in a background free Ge detector placed at its center ; the setup is located in Hall A of the Laboratori Nazionali del Gran Sasso, at a depth of 3500 m.w.e.. The 8 ^{enr}Ge + 1 ^{nat}Ge organized in 3 strings of 3 units each, are deployed at the center of the inner most shield, a volume of 64 m^3 of 5N LAr acting both as shield and as cooling medium, whose radiopurity in terms of ^{228}Th,^{238}U,^{226}Ra has been carefully studied and certified[15]. In the immediate surroundings of the detectors the amount of high Z element material, responsible for bremmstralung radiation, has been minimized to ~ 80 g of Cu/detector for detector holders. The Ge detectors are readout by a custom cryogenic, low activity (170 μBq in ^{228}Th for 3 channels), low noise front-end charge preamplifiers located in LAr at a distance of about 30 cm from the top of the detector array. The preamplifiers output analog signals are digitized, after a transmission line 20 m long 10 m of which are in LAr, by 100 MHz FADCs, with a trigger threshold of 100 keV (later 40 keV).
Each detector string is enclosed in a 60 μm thick Cu cylinder (figure 1), called minishroud to *i)* limit to a few mm from the detector surfaces the LAr volume that experience the electric field generated by the detector bias voltage, and *ii)* prevent the exchange of LAr from outside to the inside of the minishroud. A 30 μm thin copper cylinder - called radon shroud with a diameter of 75 cm encloses the detector array.
The outmost shield shell is the 590 m^3 volume of high purity (> 0.17 MΩm) water, operated as a Cerenkov veto read out by 66 PMTs against the residual muons crossing the apparatus ($\sim 1/h^{-1} \cdot m^{-2}$). The hermeticity of the muon veto is guaranteed by plastic scintillator panels located above the clean room ceiling, to veto

those muons crossing vertically the cryostat through the neck. The GERDA apparatus is fully described in [14].

2. Data taking and treatment

The exposure ($\mathscr{E}$ = detector mass · live time) smoothly built up from 9 November 2011 to 3 May 2013 in 492.3 days live time, as shown in figure 2. First an array of eight semi-coaxial (COAX) detectors for a total mass of 17.67 kg of ^{enr}Ge has been exposed. Shortly after their deployment, two detectors, for a mass of 3.045 kg, exhibited high leakeage current, hence were not included into the analysis. Another coaxial detector was lost in March 2013. To compensate their mass loss, in June 2012 five BEGE ^{enr}Ge detectors, from the pilot production of the GERDA Phase II detectors, for a mass of 3.63 kg, were added; one of them showed instabilities and therefore it has also not been included in the physics analysis. Finally the overall expsoure is of 21.6 kg·yr detector mass, corresponding to (215.2 ± 7.6) mol·yr of ^{76}Ge within the active volume has been collected.
The energy scale and the energy resolution (FWHM) are calibrated weekly irradiating the array with ^{228}Th sources. The energy reconstruction is performed off-line via a pseudo-gaussian shaping applied to the digitized waveforms. The calibration curve reproduces within 0.3 keV the observed peak positions. The energy resolution was stable over the entire data acquisition period. The gain variation between consecutive calibrations is less than 1 keV at 2614 keV, namely $5{\cdot}10^{-4}$, or < 30% of the expected FWHM at $Q_{\beta\beta}$ [14]. The electronic stability is monitored by regularly injecting charge pulses into the input of the amplifiers. The mass weighted resolution at $Q_{\beta\beta}$ derived from the ^{42}K 1525 keV γ-line, shown in figure 4, is 4.8 keV and 3.2 keV for COAX and BEGE detectors respectively, namely 10% broader than expected from calibrations data sets (4.5 keV and 2.9 keV respectively). These uncertainities and unlinearities affect the energy scale and show up when summing the spectra from various detector over the full data taking period.

The data treatment is outlined in the following and described in [18]. First quality cuts are applied (99.7% accepted for E > 500 keV), then single multiplicity (only 1 detector above the DAQ trigger) and anticoincidence within 1 μs with the muon veto detector are required. The acceptances of the two latter are (94.5 $\pm$ 0.6)% and (93.7 $\pm$ 0.6)% for E > 500 keV respectively. When considering the 100 keV energy region around $Q_{\beta\beta}$ the quality cut efficiency is unchanged within the errors while the anticoincidence efficiencies drop to (66 $\pm$ 7) % and (60 $\pm$ 7) % respectively, due to the absence of the $2\nu\beta\beta$ signal

Figure 1: Left panel: Schematic drawing of the main components of the GERDA experiment .Right panel: The three Cu minishrouds that encloses three ^{enr}Gedetector strings. For details see Ref. [14].

PoS(EPS-HEP 2013)515

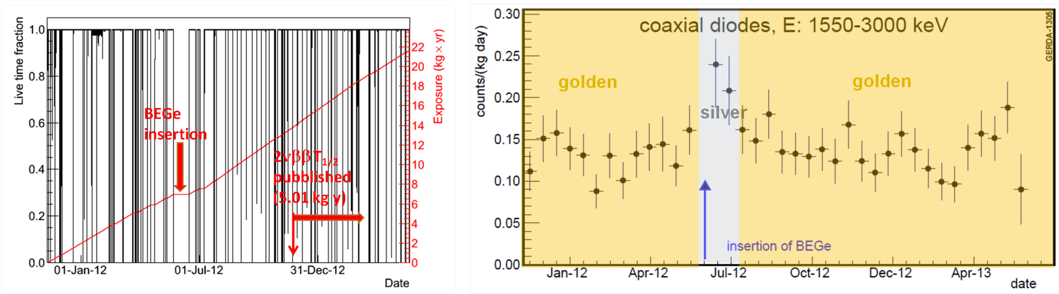

Figure 2: Left panel: The exposure ($\mathscr{E}$) build-up of the GERDA first experimental phase from November 2011 till May 2013. Right panel: the evolution of the COAXs count rate in the 1535-3000 keV energy range along the whole Phase I data taking period. The insertion of the string of BEGE detectors caused an increase of the BI due to ^{222}Rn.

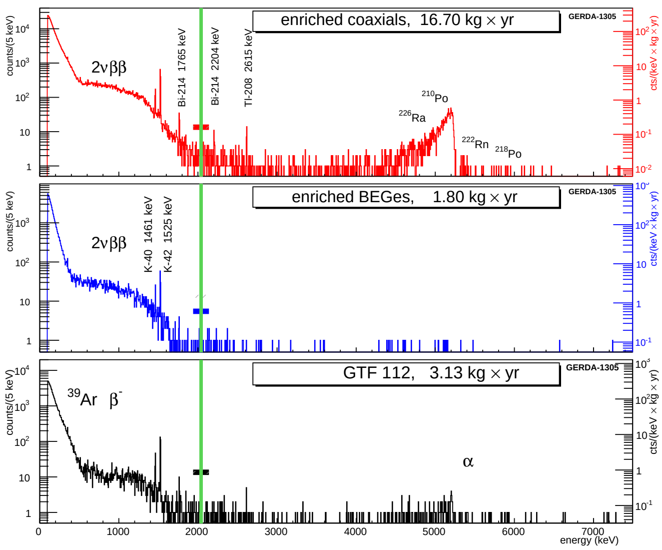

Figure 3: Energy spectra after quality, veto and anticoincidence cuts of the enriched COAX (top), BEGE (middle) and natural (bottom) data sets

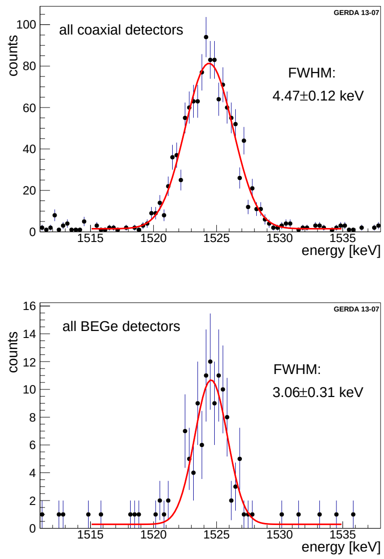

Figure 4: FWHM of the enriched COAX (top) and BEGE (bottom) data sets

(intrinsically single hit), and the drop of the full containment efficiency at the increase of the γ energy. To maximize $\mathscr{E}$ while taking advantage of the the different energy resolution, BI, and pulse shape discrimination (PSD) characterizing different detectors and time periods, data are divided in three sets (see table1): *i) golden*-COAX:$\mathscr{E}$ = 17.9 kg·yr, BI= $(1.8 \pm 2) \cdot 10^{-2}$ cts/(keV·kg·yr), are all the COAX data but two runs after the insertion of BEGE string in July 2012; *ii) silver*-COAX: $\mathscr{E}$ = 1.3 kg·yr, BI = $(6.3\ ^{+16}_{-14}) \cdot 10^{-2}$ cts/(keV·kg·yr), are the COAX data from the latter two runs; *iii)* BEGE: $\mathscr{E} \simeq 2.4$ kg·yr, BI = $(4.2\ ^{+10}_{-8}) \cdot 10^{-2}$ cts/(keV·kg·yr), are all the BEGE data. In fact BEGEs have in average 10 times lower ^{210}Po contamination and enhanced PSD features than COAXs, while the latter have a lower background index at $Q_{\beta\beta}$(prior PSD), but in the restricted period after BEGEs insertion. In the global fit to extract the $T^{0\nu}_{1/2}$, the three background indexes are free parameters. The last analisys step is the event selection based on pulse shapes, to reject background events generated by multi-site energy deposition (MSE), while preserving single-site ones (SSE): $0\nu\beta\beta$ is intrisically a SSE. The pulse shape discrimination criteria and algorithms differ for COAXs and BEGEs. For COAXs the pulse shape estimator to select SSE is the output of an Artificial Neural Network (ANN), while for BEGEs it

is the ratio of the amplitudes of current pulse vs. charge pulse (A/E). [17]: events populating the 1592 keV γ-line (double escape peak of the 2614 keV, ^{208}Tl) and the full energy peaks (FEP) of the 1620 keV ^{212}Bi γ-line are proxies of $0\nu\beta\beta$ (SSE) and background (MSE) respectively. The acceptances are then verified on other SSE classes of events, as $2\nu\beta\beta$ and Compton edges. Figure 5 show the distribution of the PSD estimator for different event classes for COAXs and BEGEs respectively. When requiring an acceptance of 90% (92%) at the DEP line for the COAXs (BEGEs), the acceptance of $\sim$ 50% ($\sim$10%) for the ^{212}Bi γ full energy peaks (FEP) is found. The PSD systematics for the SSE selection is evaluated to be 10% (2%). With the same cuts the acceptances for the $2\nu\beta\beta$ population evaluated in the energy range from 1 MeV to 1.45 MeV are (85% $\pm$ 2%) and (91% $\pm$ 5%) for COAX and BEGE respectively. The stronger MSE event rejection power of the BEGEs, reflects the larger dishomogeneities of the electric field and therefore of the drift isocrones [19]. The BEGEs acting as pulse strectcher, allow to better resolve two individual energy deposition site.
For the first time in a $\beta\beta$ decay search experiment, a blinded analysis was performed: events falling in a 40 keV region of interest (ROI) centered at $Q_{\beta\beta}$ were not reconstructed untill the described analysis cuts and algorithms, their efficiencies and systematics have been defined [20][17].

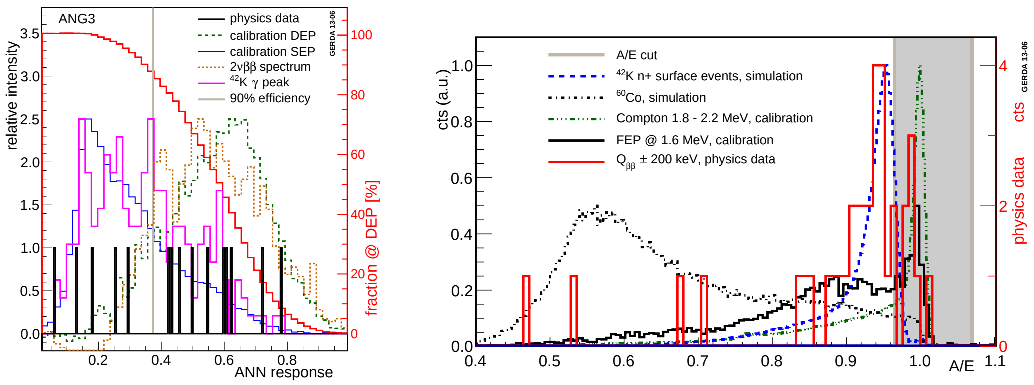

Figure 5: The distribution of the PSD estimator parameter for COAXs (left) and BEGEs (right), for several classes of events. The grey vertical line indicate the cut on the PSD parameter to accept/reject events.

Before the unblinding, a model [20] of the radiation sources and their location has been worked out. The source components, their intensity and location are identified and constrained by the characteristic γ and α-lines identified in the spectra: the model (in the following BM) well reproduces the energy spectra in almost two energy decades from 100 keV (the analysis threshold) up to 7 MeV: the *minimal* BM includes $2\nu\beta\beta$ in ^{enr}Ge, ^{39}Ar, ^{42}Ar and ^{42}K in LAr, ^{40}K in holders (H), responsible for both the continuum and the few visible γ lines up to energies of $\sim$1600 keV (see fig. 3). ^{214}Bi,^{228}Th, ^{228}Ac in detector holders, ^{214}Bi and ^{42}K βs at p$^+$ contact, ^{60}Co both in H and in detectors plus degraded alphas are the relevant components in the energy range around $Q_{\beta\beta}$ and up to $\sim$ 3 MeV (fig. 6 left panel). The α region above 3 MeV is also shown in fig. 6 right panel: it is described by ^{210}Po on detector surface, ^{226}Ra both on detector surface and in LAr. When more components, i.e. ^{228}Th from calibration source, ^{214}Bi and ^{42}K at the p$^+$ contact and ^{214}Bi in LAr, are included in the BM (*m*aximal BM), the data are also well fitted, but these extra components are not strictly required. The BM provides a solid base for the flat background hypothesys that is assumed when fitting the data.
The unblinding confirmed that no lines are present in the data within 30 keV around $Q_{\beta\beta}$. Hence it is correct to assume a flat background at $Q_{\beta\beta}$ and estimate it by a linear fit of an energy window of 230 keV, excluding the $Q_{\beta\beta}$ (2039$\pm$5) keV) and the intervals (2104$\pm$5) keV and (2119$\pm$5) keV, which contain known γ-ray peaks from ^{208}Tl and ^{214}Bi.

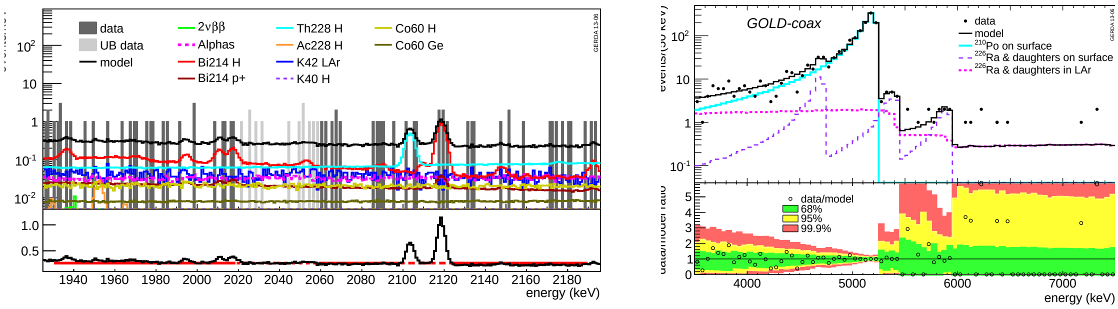

Figure 6: Left:Decomposition of the COAX data set energy spectrum. The individual components are identified by characteristic gamma ot alfa lines. Right: The energy spectrum of the *golden*-COAX and its decomposition in the α region for E > 3 Mev. Well visible are the ^{210}Po and ^{226}Ra α lines.

The half-life on $0\nu\beta\beta$ decay is derived as

$$T_{1/2}^{0\nu} = \frac{(\ln 2)\cdot N_A}{m_{enr}\cdot N^{0\nu}}\cdot\mathscr{E}\cdot\varepsilon \tag{2.1}$$

$$\varepsilon = f_{76}\cdot f_{av}\cdot\varepsilon_{fep}\cdot\varepsilon_{psd} \tag{2.2}$$

with N_A being Avogadro's constant and $m_{enr}=75.6$ g the molar mass of the enriched material. $N^{0\nu}$ is the observed number of excess counts above the background or the corresponding upper limit. The efficiency ε accounts for the fraction of ^{76}Ge atoms (f_{76}), the active volume fraction (f_{av}) [21], the signal acceptance by PSD (ε_{psd}), and the efficiency for collecting the full energy ε_{fep}. The latter is the probability that a $0\nu\beta\beta$ decay taking place in the active volume of a detector releases its entire energy in the latter, hence contributing to the full energy peak at $Q_{\beta\beta}$. Energy losses are due to bremsstrahlung photons, fluorescence X-rays, or electrons escaping the detector active volume. Monte Carlo simulations yield $\varepsilon_{fep}=0.92$ (0.90) for semi-coaxial (BEGe) detectors. Table 2 summarize all the relevant mass averaged efficiencies and parameters entering in the $T_{1/2}^{0\nu}$ computation.

3. Results and Conclusions

As reported in table 1, the unblinding revealed 5 events in the *golden*, 1 events in the *silver*, 1 event in the BEGE data sets, to be compared to the expected numbers from the flat background hypothesys, namely 5.1 in the COAX and 2.5 in the BEGEs ; the PSD rejects 3 events in the COAXs and the single event in the BEGEs. No excess of events beyond the expected background is observed in any of the three data sets. The results on $0\nu\beta\beta$ are obtained with PSD. A Profile Likelihood fit of the spectrum, shown in figure 7, is performed: the three BI (costant) and $1/T_{1/2}^{0\nu}$ (gaussian centered at $Q_{\beta\beta}$, σ = FWHM/2.35) are the 4 free parameters. The best fit returns $N^{0\nu}=0$. In a frequentist approach, this is consistent with a signal of strength $N^{0\nu}<3.5$ counts (blue solid line of figure 7), corresponding to $T_{1/2}^{0\nu}>2.1\cdot10^{25}$ yr at 90% C.L. [1]. For the claimed signal of $T_{1/2}^{0\nu}>1.19\cdot10^{25}$ yr, an excess number of 5.9 ± 1.4 counts over 2 ± 0.3 counts from background are expected (red dotted line of figure 7) in $\pm2\sigma$ around $Q_{\beta\beta}$. GERDA founds 3 counts, none of them being within $\pm1\sigma$ from $Q_{\beta\beta}$; given the exposure and the spectral distribution, the probability of observing zero excess counts in case of a true signal with the claimed half-life is 1%. When comparing by Bayes factor the *claimed signal* (H1) versus the *background only* (H0) hypothesys, one gets P(H1)/P(H0)=$2.4\cdot10^{-2}$. Hence GERDA does not confirm the claim of [7]; the evidence claimed in [8], is not considered because affected by errors in the analysis treatment as discussed in [9]. Moreover, when combining GERDA with HDM

[12] and IGEX [13] data, $T_{1/2}^{0\nu} > 3.0 \cdot 10^{25}$ yr at 90% C.L. [1] and the ratio P(H1)/P(H0) becomes $2.0 \cdot 10^{-4}$. This corresponds to m_{ee}< 0.2 -0.4 keV depending on the adopted NME$_{0\nu}$ and phase space factor.
Aiming to increase the sensitivity and to further reduce the BI of a factor 10, hence achieving 10^{-3} cts/(keV·kg·yr) at $Q_{\beta\beta}$, the GERDA apparatus will be upgraded in the next year by deploying the whole batch of freshly produced ^{enr}Ge BEGEs, and implementing LArscintillation light readout. At the restart of the physics data taking the exposed mass will be $\sim$ 40 kg of ^{enr}Ge.

Table 1: Parameters for the three data sets with and without the pulse shape discrimination (PSD). "bkg" is the number of events in the 230 keV window and BI the respective background index, calculated as bkg/($\mathcal{E}$ · 230 keV). "cts" is the observed number of events in the interval $Q_{\beta\beta}$±5 keV.

data set	$\mathcal{E}$[kg·yr]	$\langle\varepsilon\rangle$	bkg	BI †	cts
without PSD					
golden	17.9	0.688±0.031	76	18±2	5
silver	1.3	0.688±0.031	19	63^{+16}_{-14}	1
BEGe	2.4	0.720±0.018	23	42^{+10}_{-8}	1
with PSD					
golden	17.9	$0.619^{+0.044}_{-0.070}$	45	11±2	2
silver	1.3	$0.619^{+0.044}_{-0.070}$	9	30^{+11}_{-9}	1
BEGe	2.4	0.663±0.022	3	5^{+4}_{-3}	0

† in units of 10^{-3} cts/(keV·kg·yr)

Table 2: Summary of relevant parameters entering in the $T_{1/2}^{0\nu}$evaluation

Data Sets	FWHM [keV]	ROI [keV]	<$\langle f_{76}\rangle$ %	$\langle f_{av}\rangle$ %	$\langle\varepsilon_{76}\rangle$ %	$\langle\varepsilon_{PSD}\rangle$ %	$\langle\varepsilon\rangle$ %
COAX	4.8±0.2	±5	86	87	92	90^{+5}_{-9}	$61.9^{+4.4}_{-7.0}$
BEGE	3.2±0.2	±4	88	92	90	92±2	66.3±2.2

References

[1] M. Agostini *et al.*, GERDA-collaboration, Phys. Rev. Lett. **111**, 122503 (2013)

[2] M. Agostini *et al.* GERDA-collaboration, J. Phys. G **40**, 035110 (2013)

[3] F. Vissani and A. Strumia, arXiv:hep-ph/0606054v3

[4] W. Rodejohann, J. Phys. G **39**, 124008 (2012)

[5] O. Cremonesi, Proceedings of the 2013 EPS Conference.

[6] Particle Data Group, Review of Particle Physics, K. Nakamura *et al.*, J. Phys. G **37** (2010)

[7] H. V. Klapdor-Kleingrothaus *et al.*, Phys. Lett. B **586** (2004) 198

[8] H. V. Klapdor-Kleingrothaus and I.V. Krivosheina, Mod. Phys. Lett. **A21** (2006) 1547

[9] B. Schwingenheuer, Annalen der Physik **525** (2013) 269

[10] Gerda Letter of Intent

[11] G. Heusser, Annu. Rev. Part. Nuc. Sci. **45** (1995) 543

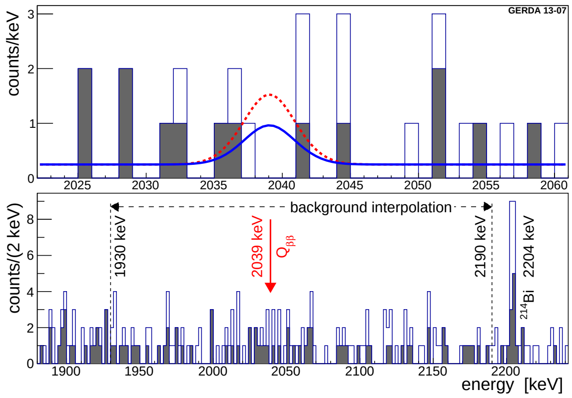

Figure 7: The combined energy spectrum from all ^{76}Ge detectors without (with) PSD is shown by the open (filled) histogram. The lower panel shows the region used for the background interpolation. In the upper panel, the spectrum zoomed to $Q_{\beta\beta}$ is superimposed with the expectations (with PSD selection) based on the central value of Ref. [7], $T^{0\nu}_{1/2} = 1.19 \cdot 10^{25}$ yr (red dashed) and with the 90 % upper limit derived in this work, corresponding to $T^{0\nu}_{1/2} = 2.1 \cdot 10^{25}$ yr (blue solid).

[12] HDM-collaboration: H. V. Klapdor-Kleingrothaus *et al.*, Eur. Phys. J. **A12** (2001) 147

[13] IGEX Collaboration: C. E. Aalseth *et al.*, Phys. Rev. D **65** (2002) 092007

[14] K.H. Ackermann *et al.*, Eur. J. Phys. C **73** (2013) 2330

[15] G. Zuzel and H. Simgen, Appl. Rad. Isot. **67** (2009) 889

[16] M. Agostini *et al.*, JINST **6** (2011) P08013

[17] M. Agostini *et al.* GERDA-collaboration, Eur. Phys. J. C **73**, 2583 (2013)

[18] M Agostini, L Pandola, P Zavarise, J. Phys. (Conf. Ser.) **368** (2012) 012047

[19] M. Agostini et al., JINST **6** (2011) P03005.

[20] M. Agostini *et al.* GERDA-collaboration, EPJC in press, arXiv:1306.5084 [physics.ins-det]

[21] M. Bernabé
Heider, PhD thesis, University of Heidelberg (2009) Comput. Phys. Commun. **180** (2009) 2197 (2012) 24